Dental Materials xxx (xxxx) xxx

Contents lists available at ScienceDirect

Dental Materials

journal homepage: www.elsevier.com/locate/dental

Novel antimicrobial and self-healing dental resin to combat secondary caries and restoration fracture

Shuo Yao [a], Ludan Qin [a], Li Ma [a], Xiaoran Zhang [a], He jiang [a], Jiajia Zhang [a], Chuanjian Zhou [b], Junling Wu [a,1,*]

[a] Department of Prosthodontics, School and Hospital of Stomatology, Cheeloo College of Medicine, Shandong University & Shandong Key Laboratory of Oral Tissue Regeneration & Shandong Engineering Laboratory for Dental Materials and Oral Tissue Regeneration & Shandong Provincial Clinical Research Center for Oral Diseases, Jinan 250012, China

[b] Research Institute of Polymer Materials, School of Materials Science and Engineering, Shandong University, Jinan 250061, China

ARTICLE INFO

Keywords:
Self-healing
Antimicrobial
Dental resin
Nanoparticles
Microcapsules
Mechanical property

ABSTRACT

Objective: Dental resin composites have been the most popular materials for repairing tooth decay in recent years. However, secondary caries and bulk fracture are the major hurdles that affect the lifetime of dental resin composites. This current study synthesized a novel antimicrobial and self-healing dental resin containing nanoparticle-modified self-healing microcapsules to combat secondary caries and restoration fracture.

Methods: Multifunctional dental resins containing 0–20% nanoparticle-modified self-healing microcapsules were prepared. The water contact angle, antimicrobial properties, mechanical properties, cell toxicity, and self-healing capability of the dental resins were tested.

Results: A novel multifunctional dental resin was synthesized. When the microcapsule mass fraction was 10%, the resin presented a strong bacteriostasis rate (80.3%) and excellent self-healing efficiency (66.1%), while the hydrophilicity, mechanical properties, and cell toxicity were not affected.

Significance: The novel antimicrobial self-healing dental resin is a promising candidate for use in clinical practice, which provides a simple and highly efficient strategy to combat secondary caries and restoration fracture. This novel dental resin also gives the inspiration to prolong the service life of dental restorations.

1. Introduction

Dental resin composites have been the most popular materials for repairing tooth decay owing to their better aesthetic property, simplicity of usage, and adequate mechanical durability [1–4]. However, catastrophic failure of resin restorations occasionally occurs because of microcrack and secondary caries [5,6]. Therefore, the short service life and potential health risks of resin materials are major drawbacks that limit their development [7]. Several techniques have been used in recent studies to extend the lifespan of dental composites, including lowering shrinkage stress and strain, raising fracture toughness, introducing self-healing capability and antimicrobial properties [7].

In the complex oral environment, dental resin composites degrade due to microcracks caused by thermal and mechanical fatigue [8,9]. Self-healing material is a type of smart material, which has the capability of automatically repairing the cracks and damage when a microcrack occurs, and its mechanisms of action include intrinsic, vascular, and microcapsule (MC)-based self-healing approaches [10–17]. Self-healing materials based on MCs are widely used and can be applied to textiles, cement-based materials, and dental resin materials, et al. [18–23]. A remedy to solve the issue of secondary caries is to develop antimicrobial dental composites [24–26]. Therefore, self-healing dental materials with antimicrobial properties have gradually attracted people's attention [1,27,28].

Wu [29] et al. developed a multifunctional dental resin by combined use of poly urea-fromaldehyde (PUF)- triethylene glycol dimethacrylate (TEGDMA) MCs and nano-silica antimicrobial filler. This novel resin combines self-healing and antimicrobial capability. As for dental resin cement, the combined application of MCs and antimicrobial filler also demonstrated promising self-healing and antimicrobial capability [30]. Furthermore, an innovative dental resin material with the abilities of self-healing, antimicrobial, and remineralization was developed by Wu

* Corresponding author.
E-mail address: doctorwujunling@163.com (J. Wu).
[1] Present/permanent address: No.44–1 Wenhua Road West, 250012, Jinan, Shandong, China.

https://doi.org/10.1016/j.dental.2023.09.009
Received 1 June 2023; Received in revised form 3 August 2023; Accepted 24 September 2023

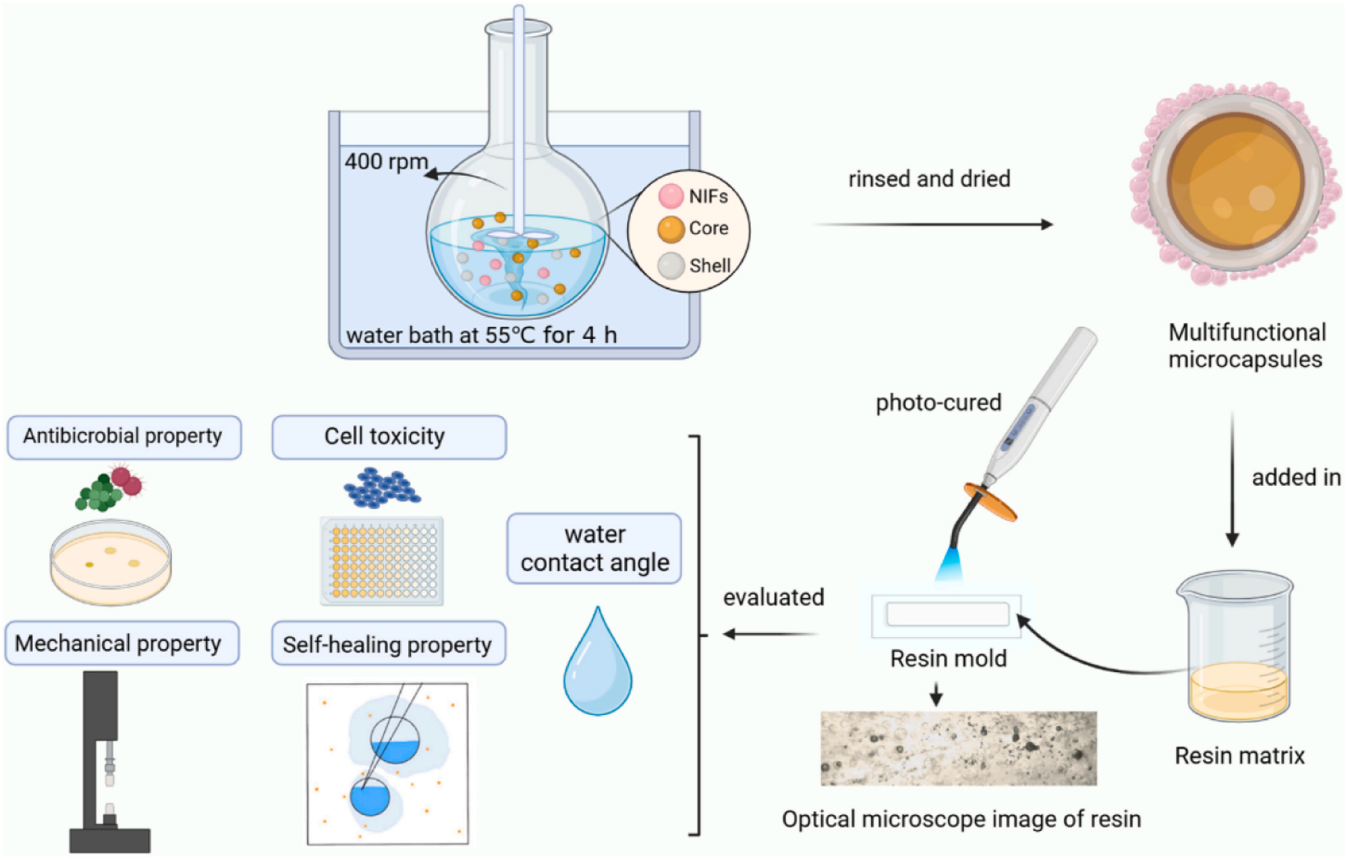

Fig. 1. - Schematic diagram of the study.

[27] et al. PUF-TEGDMA MCs, dimethylaminohexadecyl methacrylate, and amorphous nanoscale calcium phosphate were added in this dental composite resin material. This method can also be applied to dental adhesive resin [31]. Chen [32] et al. synthesized a dental resin composite containing self-healing PUF-TEGDMA MCs and protein-repellent 2-methacryloyloxyethyl phosphorylcholine (MPC) to combat bulk fracture and secondary caries. This method is a promising strategy to improve the longevity of resin composites. Ahangaran [33] et al. added poly (methyl methacrylate) (PMMA) MCs and silica nanoparticles into dental composites. The experimental results showed that the dental nanocomposite demonstrated excellent antimicrobial and self-healing capability.

However, the construction of multifunctional dental materials requires the addition of multiple functional substances. The operation is complicated, and excessive additives could alter the resin's inherent qualities. On the other hand, the polymer substance used to create the MCs' shell is typically fragile, and during processing, the MCs might break [34]. Various methods, such as preparing multilayered structured MC, increasing the thickness of the shell layer, and introducing inorganic material into the shell, have been used to enhance MCs [35–37]. A sturdy capsule shell could avoid unnecessary MC loss during a self-healing resin's preparation [38].

To solve the above problems, a novel nano-antibacterial inorganic filler (NIF)-modified multifunctional MC with antimicrobial and self-healing capability was first synthesized [38]. Long chain Quaternary ammonium salt (QAS) was attached to nano-silica to develop the NIFs. QAS, one of the immobilized antimicrobial agents, could kill the adhered bacteria directly by lysing the bacteria and exhibited long-term antimicrobial properties [24,25,39–47]. Meanwhile, the nano-silica could enhance the strength of MCs. These self-healing MCs have robust hybrid shells, strong bactericidal action against oral bacteria, great self-healing capability, low toxicity, and can disperse well in the dental resin [38]. The properties of these multifunctional MCs were characterized in our previous research [38]. The performance of this novel type of MC in a dental resin is awaiting continuous exploration.

This work develops a novel dental resin containing these self-healing MCs with NIFs, and their hydrophilicity, antimicrobial properties, mechanical properties, cell toxicity, and self-healing capability were investigated to guide future practical clinical applications. Meanwhile, the optimum amount of MCs was first investigated to ensure that the resin has good antimicrobial and self-healing capability without compromising mechanical properties and cell toxicity. Different from previous studies, resin merely containing the novel MCs could achieve multiple functions. Moreover, this strategy could also apply to other dental materials like dental adhesive and luting cement. We expect this novel multifunctional resin could provide a possible method to combat secondary caries and restoration fracture and give the inspiration to prolong the service life of dental restorations.

2. Materials and methods

2.1. Materials

Ammonium, benzoyl peroxide (BPO), bisphenol A glycidyl dimethacrylate (BisGMA), chloride, formaldehyde solution (37 w/v %), N, N-dihydroxyethyl-p-toluidine (DHEPT), urea, TEGDMA, phenyl bis (2,4,6-trimethyl benzoyl) phosphine oxide (BAPO), and resorcinol were obtained from Macklin Biochemical Co., Ltd. Ethylene maleic anhydride was obtained from Sigma. 4% paraformaldehyde was obtained from Biosharp. Penicillin/streptomycin was obtained from EveryGreen. Human gingival fibroblasts (HGFs) were selected as experimental cells for cytotoxicity experiments and were provided by Shandong Key Laboratory of Oral Tissue Regeneration. Fetal bovine serum was obtained from Gibco. Cell counting kit-8 (CCK-8) was obtained from Dojindo.

Table 1
MCs and NIFs wt% in the self-healing dental resin.

Groups	Microcapsules (wt%)	NIFs (wt%)
M_0	0	0
M_5	5	0
M_{10}	10	0
M_{15}	15	0
M_{20}	20	0
N_{10}	0	10

Dimethyl sulfoxide (DMSO) was obtained from Solarbio. Dulbecco's modified Eagle's high glucose medium was obtained from HyClone. A viability/Cytotoxicity Kit for bacteria cells was obtained from APB Biosciences. *Streptococcus mutans* (*S. mutans*, ATCC 25175) were obtained from Shandong Key Laboratory of Oral Tissue Regeneration. Brain heart infusion broth (BHI) was obtained from Hope biotechnology. All materials were of analytical grade and were applied without further purification.

2.2. Preparation of multifunctional MC with NIFs

The schematic diagram of the study was shown in Fig. 1. NIFs were prepared via a protocol similar to our previous study [38]. 1 wt% DHEPT was added to 30 mL of TEGDMA. Distilled water (50 mL) and ethylene maleic anhydride aqueous solution (2.5 wt%, 15 mL) were incorporated to a round bottom flask with a mechanical stirrer. Then, add urea (1.5 g), resorcinol (0.15 g), and ammonium chloride (0.15 g) into the flask while being heated in a water bath at 400 rpm. Adjusted pH to 3.5 and added TEGDMA-DHEPT liquid into the flask. Added 3.78 g formaldehyde solution and 0.378 g NIFs to the flask, and reacted at 55 °C for 4 h. Distilled water was used to rinse and filter the MCs. Air dried 24 h at room temperature to obtain white powdered MCs.

2.3. Characterization of multifunctional MC with NIFs

The formation process and size distribution of MCs were recorded by optical microscopy (Olympus IX73, Japan). The morphology of MCs was characterized by field emission scanning electron microscopy (FE-SEM) (Carl Zeiss G300, Germany). The roughness of MCs was characterized by an atomic force microscope (AFM) (Bruker Bioscope Resolve, Germany) of tapping mode. The Fourier transform infrared (FTIR) spectrometer (Bruker Optik, Germany) was used to obtain FTIR spectra of MCs via the KBr method.

2.4. Preparation of the antimicrobial self-healing dental resin containing multifunctional MCs

The resin was prepared from TEGDMA monomers and BisGMA at 1:1 mass ratio, supplemented with 0.5 wt% BPO and 1 wt% BAPO. The dental resin containing 0 wt%, 5 wt%, 10 wt%, 15 wt%, and 20 wt% MCs (denoted as M_0, M_5, M_{10}, M_{15}, and M_{20}, respectively) were prepared, as shown in Table 1. The resin without MCs served as the negative control group. According to previous research and preliminary experimental results, NIFs had strong antimicrobial properties, and the resin containing 10 wt% NIFs could achieve great antimicrobial properties. Therefore, a positive control group containing 10 wt% NIFs (denoted herein as N_{10}) was also set up. The specimens were placed in the mold (the specific dimensions are indicated in the following experiments) and photo-cured on every side for 1 min. After curing, the sharp edges of the samples were smoothed with abrasive paper. Before antimicrobial and cytotoxicity testing, all samples were sterilized by ultraviolet (UV) irradiation 2 h per side. All samples for mechanical and self-healing testing were kept for 24 h at 37 °C in distilled water.

2.5. The water contact angle of the resin

The multifunctional dental resin specimens of M_0, M_5, M_{10}, M_{15}, and M_{20} were prepared as resin discs (with diameter × thickness = 10 × 3 mm). The contact angle analyzer (DSA100S) (Kruss, Germany) was used to characterize the water contact angle (WCA) by using a 2 μL of deionized water. The results were the average value obtained from six measurements at a test temperature of approximately 25 °C.

2.6. Bacterial growth on material surfaces

S. mutans was cultured under anaerobic conditions at 37 °C. Then, the optical density (OD) of *S. mutans* suspension was adjusted to 0.5 at 600 nm. The resin specimens (with diameter × thickness = 10 × 3 mm) of the M_0, M_{10}, M_{20}, and N_{10} groups, 2 mL sterile BHI broth, and twenty microliters of *S. mutans* suspension were placed in a 24-well plate. After incubation for 24 h, bacteria were collected by sonication and vortex mixing the resin disk in 2 mL BHI for 3 min. Serially diluted bacterial samples were distributed on BHI agar plates for a 24-hour incubation and quantified the number of CFU recovered (n = 3). The bacteriostasis rate (R) was calculated using Eq. (1):

$$R \quad (\%) = [(N_{control} - N_{test})/N_{control}] \times 100\% \tag{1}$$

$N_{control}$ and N_{test} indicate the number of colonies in the control and experimental groups.

2.7. SEM observation

2 mL BHI, 20 μL of *S. mutans* suspension, and resin specimens of the M_0, M_{10}, M_{20}, and N_{10} groups were placed in a 24-well plate. After incubation for 24 h, specimens were washed with PBS and fixed in 4% paraformaldehyde. Then, dried in a critical point drier (Leica EM, Switzerland) after being dehydrated with gradient ethanol. The samples were observed by SEM (Phenom Pro, The Netherlands) after gold sputtering.

2.8. Live/dead bacterial staining

Resin specimens were prepared as described in the SEM observation. Specimens were rinsed with sterile saline to remove loose bacteria after 24 h incubation. A viability/Cytotoxicity Kit for bacteria cells was used to stain for live and dead bacteria following the manufacturer's protocol. Fluorescent photographs of the samples were obtained by a fluorescence microscope (Leica D-35578, Germany). Live bacteria produced green fluorescence, and dead bacteria produced red color.

2.9. Bacterial metabolic activity

Resin specimens were prepared as described in the SEM observation. The bacterial suspensions from specimen surfaces were obtained and transferred to a 96-well plate. Added 20 μL CCK-8 to each well following the instructions of manufacturer. Evaluated the absorbance at 450 nm wavelength after incubation in the dark for 2 h. A higher absorbance value indicated a higher bacterial metabolic activity.

2.10. Flexural testing

The flexural strength (S) and elastic modulus (E) were analyzed by a universal testing machine (UTM) (Suns UTM4203, China) in three-point flexure following a previous study [38]. The resin bars (with width (b) × thickness (h) × length= 2 mm × 2 mm × 25 mm) of M_0, M_5, M_{10}, M_{15}, and M_{20} groups were fractured while being wet (n = 6). The results were calculated using Materials Test 4.0 software by Eq. (2) and Eq. (3):

$$S = 3P_{max}L/(2bh^2) \tag{2}$$

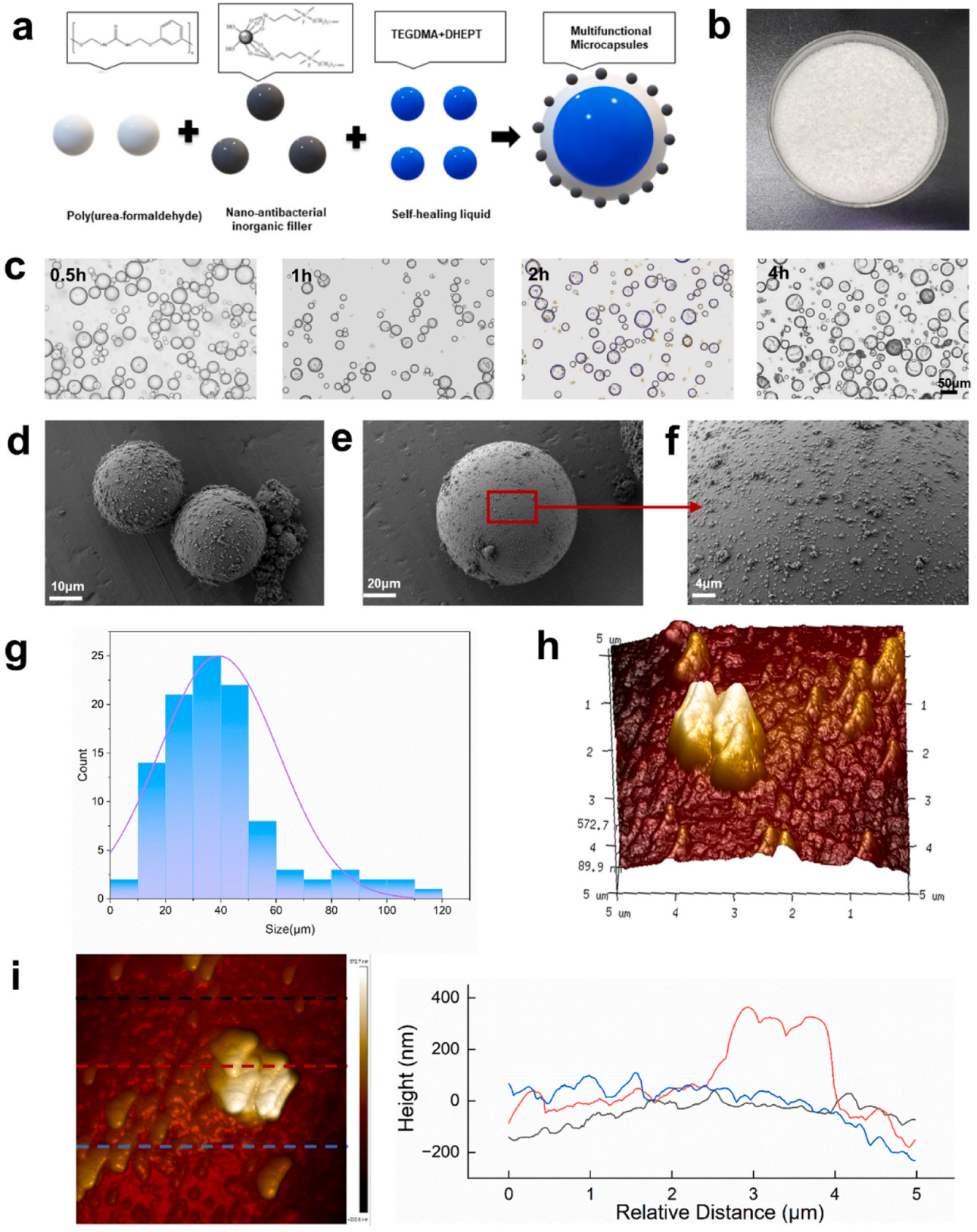

Fig. 2. Characteristics of MCs. (a) Illustration of the multifunctional MC. (b) Photograph of MCs. (c) The formation process of MCs under optical microscopy. (d-f) SEM images of the MC. (g) The size distribution of MCs. (h) 3D AFM image of MC. (i) Height analyses among three straight lines in AFM surface topography image of MC.

$$E = (P/d)(L^3/[4bh^3]) \quad (3)$$

P_{max}, L, P, and d indicate the load-at-failure, span, load, and slope.

2.11. Cytotoxicity testing

Fibroblast culture medium (FM) containing penicillin/streptomycin (1%), fetal bovine serum (10%), and dulbecco's modified Eagle's high glucose medium (89%) were prepared. After UV irradiation, six M_{10} resin disks (with diameter × thickness = 8 × 0.5 mm) were immersed in 10 mL FM. Obtained resin eluents after 24 h at 37 °C and diluted to 32-, 64-, and 128-fold. HGFs (5000 cells/well) were infused onto a 96-well plate. After being cultivated at 37 °C for 24 h in an incubator with 5% CO_2, HGFs were treated with diluted resin eluents for 24 h. Set up a negative control group containing FM merely and a positive control group with 5% DMSO and FM. CCK-8 was used to evaluate the cell cytotoxicity following the manufacturers' instructions. Evaluated the absorbance at 450 nm wavelength using Eq. (4). Cell morphology was obtained using an optical microscope. The Relative proliferation rate (RPR) was calculated using Eq. (4):

$$RPR \quad (\%) = [(OD_a - OD_0)/(OD_{con} - OD_0)] \times 100\% \quad (4)$$

Where OD_a, OD_{con}, and OD_0 represent the absorbance of experiment groups, the negative control group, and the blank groups without cells.

2.12. Self-healing capability testing

M_{10} dental resin was selected for self-healing capability testing. In the preliminary experiment, the M_{10} group not only had strong antimicrobial properties but also showed no significant differences from the M_0 group in mechanical properties. Following previous studies [38], six resin bars (2 mm × 2 mm × 25 mm) were prepared to measure the fracture toughness. The resin bar was machined with a notch (500 μm depth) using a diamond blade. The notch was then further deepened with a razor blade, to a total depth of around 700–800 μm. The original K_{IC} (noted as $K_{IC\text{-}virgin}$) was measured using UTM (span = 10 mm, crosshead speed = 0.5 mm/min) via the single edge V-notched beam method. Then, the fractured specimens were put back into the mold right away and kept in an incubator (37 °C). After 24 h, the same three-point fixture was used to test the healed specimens and obtained $K_{IC\text{-}healed}$ using Eq. (5). Fractured surfaces were observed using FE-SEM (JSM-7800 F, JOEL, Japan). The Self-healing efficiency (η) was calculated using Eq. (5):

$$\eta = (K_{IC-healed}/K_{IC-virgin}) \times 100\% \quad (5)$$

2.13. Statistical analysis

The statistical analysis was performed via the GraphPad Prism program. Mean ± SD was used to express the experiment's average values. The differences between multiple groups were analyzed using one-way analysis of variance or student's t-test.

3. Results

3.1. Characterization

Fig. 2a illustrated the structure of MCs. The gross appearances in Fig. 2b showed MCs were obtained as white powders. Fig. 2c illustrated the formation process of MCs under optical microscopy. Representative SEM images (Fig. 2d-f) demonstrated the typical spherical form of the MCs, with the deposition of NIFs and PUF nanoparticles on the shells. The diameter of MCs was 39.2 ± 21.5 μm and the size distribution was shown in Fig. 2 g The 3D AFM image of MC was shown in Fig. 2 h. Fig. 2i showed the AFM surface topography image and height analyses of MC,

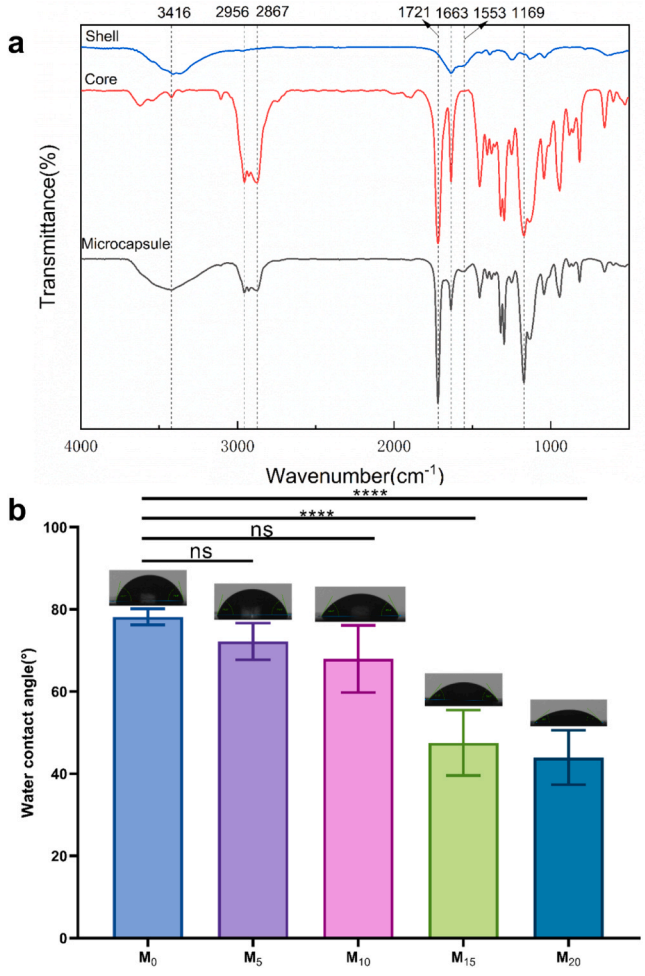

Fig. 3. The FTIR spectra of MCs and the WCA results of resin. (a)The FTIR spectra of pure TEGDMA, the PUF shell, and multifunctional MCs. (b) The WCA results of multifunctional resin. (Error bars stands for mean ± SD.*: p-value < 0.05, **: p-value < 0.01, ***: p-value < 0.001, and ****: p-value < 0.0001).

and the value of the root-mean-square roughness (R_q) was 117 nm. Due to the deposition of NIFs, the MC surface exhibited moderate undulations.

The FTIR spectra of pure TEGDMA, the MC shell, and the multifunctional MCs were shown in Fig. 3a. In the FTIR spectrum of TEGDMA, the O-H stretching vibration appeared at 3416 cm^{-1}. The peaks of 2867 and 2956 cm^{-1} indicated the C-H stretching vibration. Signal peaks that appeared at 1721, 1663, and 1169 cm^{-1} represented C═O, C═C, and C-O stretching vibration. For the MC shell, the N-H stretching vibration appeared at 1553 and 3416 cm^{-1}. The peaks of 1663 cm^{-1} represented C═O stretching vibration.

Fig. 3b showed the results of WCA of M_0, M_5, M_{10}, M_{15}, and M_{20} groups. As the amount of MCs increased, the WCA of resin increased progressively. The WCA of M_0, M_5 and M_{10} is 78.2 ± 2.0°, 72.2 ± 4.5° and 68.0 ± 8.2°. There were no discernible differences between the M_0, M_5, and M_{10} groups. When the content of MCs increased to 15 wt%, the WCA of resin significantly decreased. The WCA of M_{15} and M_{20} were 47.5 ± 8.0° and 44.0 ± 6.6°.

3.2. Bacterial growth on material surfaces

The antimicrobial properties of M_0, M_{10}, M_{20}, and N_{10} resins were shown in Fig. 4. The photographs of the culture plates were shown in Fig. 4a. The white dots on the plates represented surviving bacterial colonies. Compared with M_0, the bacterial growth in other groups were

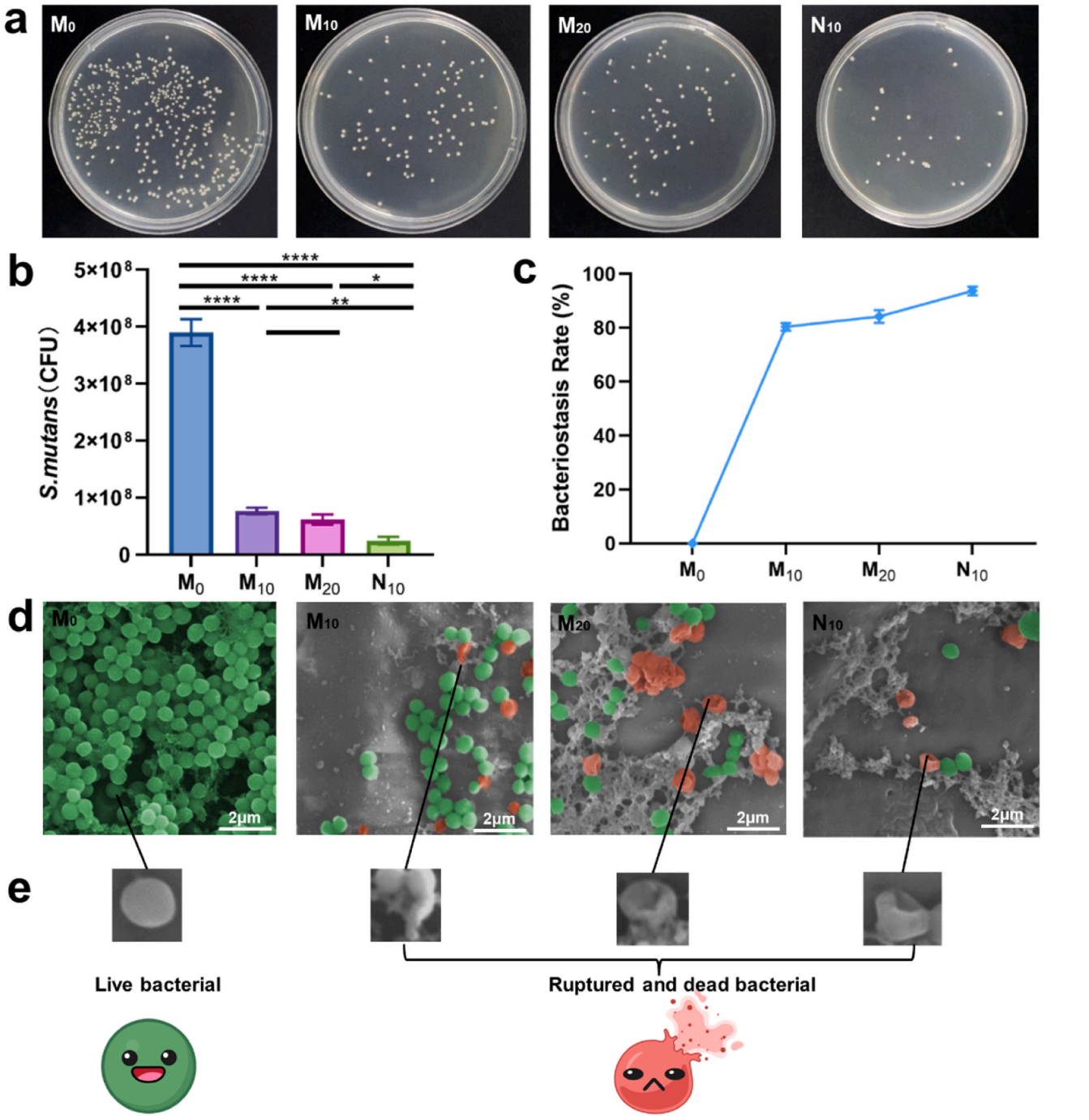

Fig. 4. Antimicrobial results. (a) Photographs of agar culture plates after culture with M_0, M_{10}, M_{20}, and N_{10}. (b) The number of bacterial colonies in different groups according to the CFU count. (c) Bacteriostasis rate of different groups. (d) Representative SEM images of S. mutans on M_0, M_{10}, M_{20}, and N_{10} surfaces. (e) The high magnification SEM images of bacteria and diagrams of intact and ruptured bacteria. (Error bars stands for mean ± SD.*: p-value < 0.05, **: p-value < 0.01, ***: p-value < 0.001, and ****: p-value < 0.0001).

significantly suppressed (P-value < 0.05) (Fig. 4b). M_0 had the highest CFU value of 3.9×10^8. As the content of MCs increased, the antimicrobial activity increased, from 7.7×10^7 CFU (M_{10}) to 6.2×10^7 CFU (M_{20}). The positive control group showed the lowest CFU value of 2.5×10^7 CFU (N_{10}). The bacteriostasis rate of M_0, M_{10}, M_{20}, and N_{10} resins were 0%, 80.3%, 84.2% and 93.7%, respectively (Fig. 4c). N_{10} showed the strongest antimicrobial properties.

SEM images revealed the morphology of *S. mutans* in different groups (Fig. 4d). The green color represents the live bacteria, and the red color represents the dead bacterial. In the control group, significant *S. mutans* with normal morphology aggregated on the surface of M_0 resin. As the content of MCs increased, the number of *S. mutans* gradually decreased, and the number of dead bacteria gradually increased. As indicated by the red color, the cell membranes of dead bacteria were destroyed, showing a pit-like shape, and the lysed cells lost their standard shapes. High-magnification SEM images of bacteria and diagrams of intact and ruptured bacteria were shown in Fig. 4e.

3.3. Live/dead bacteria staining

Fig. 5a showed the fluorescence microscopy images of different groups. The results confirmed the poor antimicrobial properties of M_0

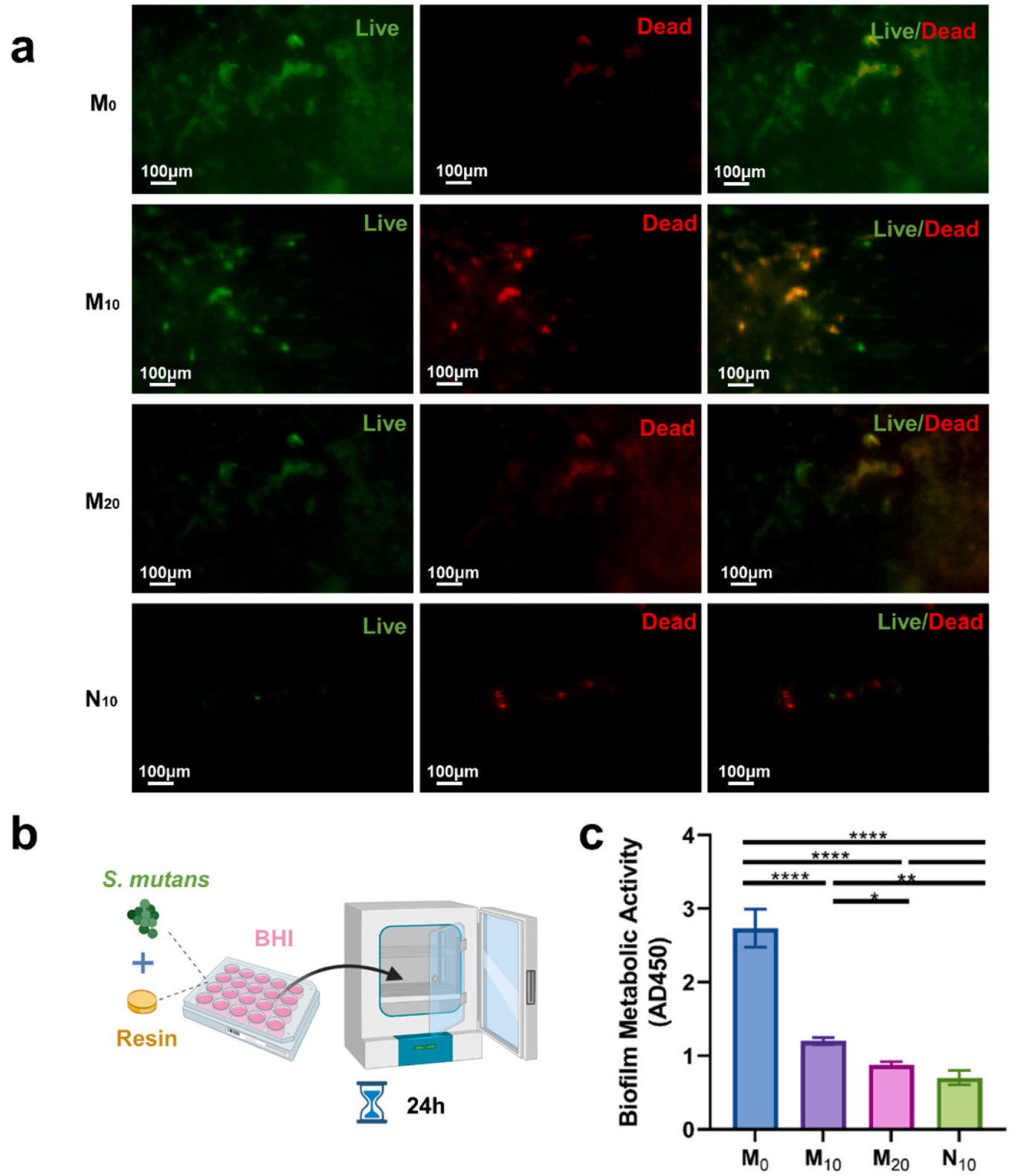

Fig. 5. Fluorescence images and metabolic activity of *S. mutans*. (a) Fluorescence images of M_0, M_{10}, M_{20}, and N_{10}. (b) Schematic diagram of a co-culture of bacteria with resin specimen. (c) Metabolic activity in biofilms on resin surfaces. (Error bars stands for mean ± SD.*: p-value < 0.05, **: p-value < 0.01, ***: p-value < 0.001, and ****: p-value < 0.0001).

with lots of live bacteria covering the resin surface. In contrast, the experimental group (M_{10}, M_{20}) had more red fluorescence, indicating strong antimicrobial properties. Some cells both stained green and red color indicated the bacterial cells were disrupted or lysed. N_{10} group showed the lowest green fluorescence and best antimicrobial properties. These results were also consistent with the results of the above experiments. Fig. 5b depicted the schematic diagram of the co-culture of bacteria and resin specimens.

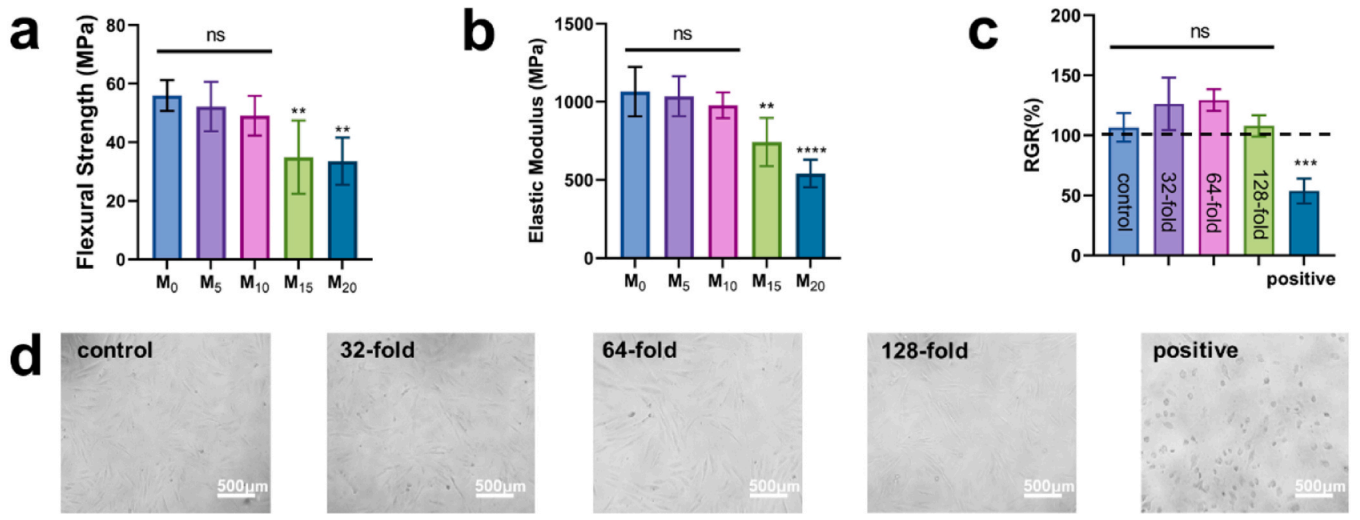

Fig. 6. Mechanical properties and cell toxicity results. (a) Flexural strength of resins. (b) Elastic modulus of resins. (c) Cell viabilities of different groups. (d) Cell morphology of different groups. (Error bars stands for mean ± SD.*: p-value < 0.05, **: p-value < 0.01, ***: p-value < 0.001, and ****: p-value < 0.0001).

3.4. Bacterial metabolic activity

Fig. 5c showed the bacterial metabolic activity data on the surfaces of specimens. The experimental results showed that the metabolic activity of bacteria decreased with an increase in the added amount of MCs. The addition of antimicrobial agents significantly affected the *S. mutans'* metabolic activity (p-value < 0.05). M_0 showed the highest absorbance values, indicating the most outstanding levels of bacterial metabolic activity. The positive control group (N_{10}) showed the lowest absorbance values and exhibited the most potent antimicrobial properties. These results were consistent with previous results.

3.5. Flexural testing

Fig. 6a showed the results of flexural strength of M_0, M_5, M_{10}, M_{15}, and M_{20} groups: 56.0 ± 5.3 MPa, 52.2 ± 8.4 MPa, 49.1 ± 6.6 MPa, 34.9 ± 12.5 MPa, and 33.5 ± 8.0 MPa. Fig. 6b showed the results of elastic modulus of M_0, M_5, M_{10}, M_{15}, and M_{20} groups: 1065.1 ± 158.5 MPa, 1035.6 ± 127.6 MPa, 977.9 ± 82.0 MPa, 742.3 ± 154.4 MPa, and 540.9 ± 88.1 MPa. The results of M_5 and M_{10} were not significantly different from M_0 (p-value > 0.1). However, the corresponding values were significantly lower in M_{15} and M_{20} compared with M_0 (p-value <0.05).

3.6. In vitro cytotoxicity of resin

As shown in Fig. 6c, the RGR of the three experimental groups exceeded 100%. Compared to the control group, all experimental groups showed similar RGR, indicating that the multifunctional resins had no obvious cytotoxicity on HGFs cells. However, the cell morphology of experiment groups displayed the same long fusiform shape as the control group, presenting well cell viability (Fig. 6d). The cells in the positive control group lost their characteristic shape (Fig. 6d) and displayed high levels of cell toxicity.

3.7. Self-healing capability testing

The self-healing properties of the resin were evaluated by the single edge V-notched beam method. Fig. 7a schematically illustrates the self-healing principle of the resin. The yellow dots represent the catalyst, the blue parts represent the self-healing monomer, and the black circles represent MCs. The yellow color in SEM image represents the resin matrix, and the blue color represents the MCs. Fig. 7bc displayed a representative fracture surface of M_0 and M_{10}. In M_0 group (Fig. 7b), the SEM image of the fracture of the neat resin was smooth and mirror-like. No self-healing MCs have been added to the M_0 group. In the M_{10} group (Fig. 7c), intact MCs, pores containing irregular MC and polymer films and layers were observed. Fig. 7d showed the two fractured halves of M_{10} specimens that were successfully bonded together after 24 h. Fig. 7e showed the self-healing efficiency of M_0 (0%) and M_{10} (66.1%).

4. Discussion

The present study first synthesized a novel type of dental resin containing MCs with NIFs, which exhibited strong antimicrobial and self-healing capability, and investigated the optimal content of MCs. Under optical microscopy, the core material was successfully encapsulated by the shell material, forming a spherical MC structure, and the thickness of the shell increased along with time [5,33]. The synthesized MCs were white powdery substances. Under the electron microscope, the MCs were completely spherical, and the surface was moderately undulating. The roughness of the MC surface was critical for forming mechanical interlock [5]. When cracks appeared, this interlocking between the resin and MC interface facilitated the rupture of the MCs. The spectra of MCs both exhibited the distinctive peaks of TEGDMA (core materials) and PUF (shell materials), indicating the TEGDMA was successfully encapsulated in MCs [33,38,48].

The wettability of the surface of the resin material can affect the actual effect when applied in a dental environment. The outcomes showed that the resin's hydrophilicity was improved by the addition of MCs. As the amount of MCs increased, the WCA of resin increased progressively. When the mass fraction of MCs was less than 10%, there was no statistically significant difference in resin surface hydrophilicity with and without MCs. However, when the mass fraction of MCs reached 15% and above, the hydrophilicity of the resin surface was significantly improved. The rough surface of MCs could improve their hydrophilicity. The increase in hydrophilicity was beneficial to improve the contact interface between resin and dentin tissue [49–51].

S. mutans was used to evaluate the antimicrobial properties of the multifunctional resin[52,53]. This novel dental resin prevented *S. mutans* from growing on its surface, and the antimicrobial properties of the resin was enhanced with the addition of MCs. SEM observation, live/dead staining, and bacterial metabolic activity provided insights into the number and viability of bacteria on the resin surfaces [28]. An intact bacterial biofilm formed on the resin surface in the control group without MCs. The bacteria were numerous in number, active, and

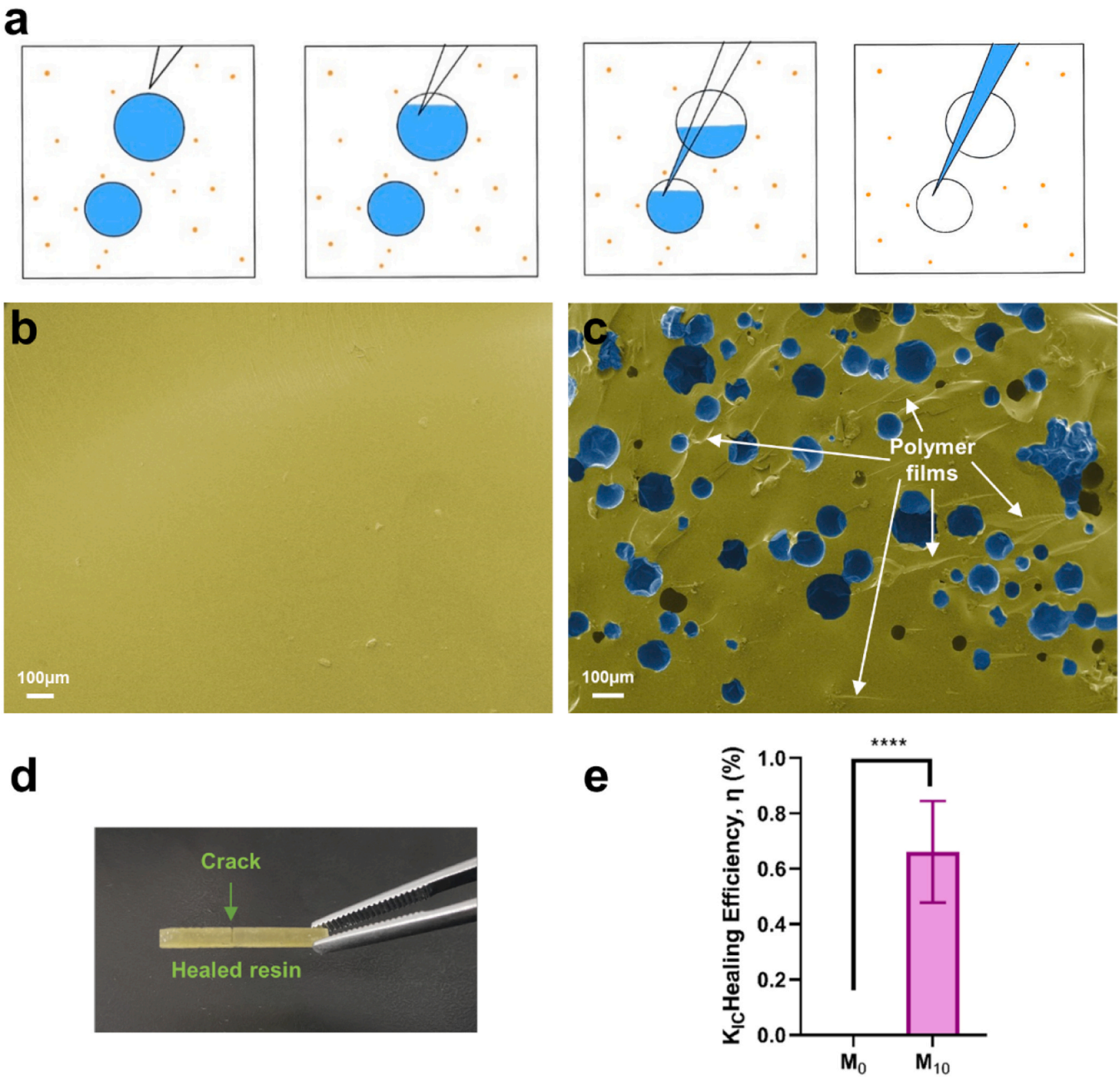

Fig. 7. Self-healing capability. (a) Illustration of the self-healing principle. (b) Representative SEM images of M_0 fractured planes. (c) Representative SEM images of M_{10} fractured planes. White arrows represent polymer films after self-healing. (d) Photograph of M_{10} resin after self-healing. The green arrow indicates the original fracture. (e) Self-healing efficiency of M_0 and M_{10}. (Error bars stands for mean ± SD.*: p-value < 0.05, **: p-value < 0.01, ***: p-value < 0.001, and ****: p-value < 0.0001).

morphologically intact. With the addition of MCs, biofilm formation on the resin surface was inhibited, the number of bacteria was decreased, the activity was decreased, and more bacteria lost their membrane integrity. NIFs resin significantly decreased the amount of bacteria in the positive control group, and there were particularly few bacteria with intact morphology. These groups responded well to the trend of increasing antimicrobial effect with increasing concentration of MCs. These manifestations were consistent with the bactericidal mechanism of QAS. When bacteria contacted the antimicrobial resin surface, the negatively charged bacteria were in contact with the positively charged quaternary amine nitrogen of QAS and disturbed the electrical balance of the membrane. Then, the change in osmotic pressure may rupture the bacterium[54]. Otherwise, long-chain QAS could penetrate bacterial cells, disrupting cell membranes like a needle piercing a balloon. Once the cell membrane was destroyed, the intracellular components of bacteria leaked out [54–56].

The flexural strength test could predict material behavior under chewing loads [5,55,57]. The MCs could be uniformly distributed in the resin matrix when the content of MCs is low. However, the high content of MCs seriously affected the dispersion of microcapsules and caused large defects inside the resin. On the other hand, adding MCs with liquid cores to the resin material was equivalent to introducing a weak part therein [58], especially at the interface between the resin matrix and MC shell [59]. The three-point bending test results showed that adding MCs up to 15% decreased the mechanical properties of the resin. As a result, the content of MCs in dental resin had an impact on its mechanical characteristics. It is still necessary to discuss and explore novel approaches to accomplish the coexistence of a high self-healing rate with

high mechanical qualities.

For dental materials, biocompatibility is an essential condition for oral applications. To simulate the oral saliva flow of patients with decreased and normal saliva, the resin eluents were diluted to 32, 64, and 128 times [5]. The results of RGR and the cell morphology of experiment groups were similar to control group, demonstrating low cell toxicity and good application prospects.

The SEM image of the fracture of the neat resin was smooth and mirror-like, which was typical of a cleavage-like brittle fracture. No self-healing MCs have been added to the M_0 group, so the self-healing efficiency is 0. In contrast, the resins in M_{10} group showed great self-healing efficiency and the ruptured resin bar were successful rebonded. The damaged event causes crack formation. When microcracks occur and pierce the MCs, TEGDMA flows to the cracks through capillary action. Moreover, the comparatively low viscosity of the healing liquid TEGDMA enables flows and fills the cracks. Through the use of a tertiary amine accelerator and a peroxide initiator, TEGDMA can form polymer through free-radical initiation; thus, bonding the crack together [38,60]. In SEM image, the healed fracture surface showed numerous layers and polymer films (white arrows), indicating that the M_{10} resin could provide a sufficient healing liquid to heal the fractured plane, rebonded, and realized the ideal self-healing efficiency [33,54,61,62]. The ideal self-healing efficiency may be related to the increased roughness and strength of the shell of MCs. The rough surfaces facilitated mechanical interlock and promoted MCs rupture. Meanwhile, the sturdy shell reduced the loss of MCs during preparation.

An insufficient dosage of MCs leads to lower self-healing efficiency. However, superabundant MCs could also lead to poor mechanical properties. In addition, some intact MCs did not break at the cracked interface, and the self-healing effect was not exerted. In future research, the number of unruptured MCs should be reduced by various methods, such as strengthening the connection between the MCs and matrix and adjusting the mechanical strength of the MC walls to be optimal for rupture.

The multifunction dental resin has excellent potential to extend the dental restoration's lifetime and combat secondary caries and restoration fracture in a relatively simple method. Different from traditional MCs, nanoparticle-modified MCs have coarse shells and antimicrobial properties. Resin merely containing the multifunctional MCs could achieve strong antimicrobial properties, excellent self-healing capability, and low cell toxicity. Therefore, the development of the novel multifunctional resin provides a possible method to prolong the service life of dental resins.

5. Conclusions

In summary, a novel multifunctional dental resin was first synthesized. This dental resin contained self-healing MCs with NIFs, which strengthen the shells of MCs and endow them with antimicrobial properties. When the MC mass fraction was 10%, the dental resin exhibited good antimicrobial properties, low cell toxicity, excellent self-healing capability, and hydrophilicity and mechanical properties were not affected. This novel dental resin could deal with the clinical challenges of secondary caries and bulk fracture, showing a promising clinical application prospect in extending the service life of resin restorations. However, the resin will endure continuous pressure from the masticating action in a complex oral environment, and further research must be done to determine how the MCs alter the dynamic mechanical properties of the dental resin.

Declaration of Competing Interest

The authors declare no conflict of interest.

Acknowledgements

This work was supported by the National Natural Science Foundation of China (Grant No. 82071165).

References

[1] Yao S, Li T, Zhou C, Weir MD, Melo MAS, Tay FR, et al. Novel antibacterial and therapeutic dental polymeric composites with the capability to self-heal cracks and regain mechanical properties. Eur Polym J 2020;129:109604.
[2] Wu J, Xie X, Zhou H, Tay FR, Weir MD, Melo MAS, et al. Development of a new class of self-healing and therapeutic dental resins. Polym Degrad Stabil 2019;163:87–99.
[3] Bayne SC, Ferracane JL, Marshall GW, Marshall SJ, van Noort R. The evolution of dental materials over the past century: silver and gold to tooth color and beyond. J Dent Res 2019;98:257–65.
[4] Fugolin APP, Pfeifer CS. New resins for dental composites. J Dent Res 2017;96:1085–91.
[5] Wu J, Weir MD, Zhang Q, Zhou C, Melo MA, Xu HH. Novel self-healing dental resin with microcapsules of polymerizable triethylene glycol dimethacrylate and N,N-dihydroxyethyl-p-toluidine. Dent Mater 2016;32:294–304.
[6] Wu J, Zhou C, Ruan J, Weir MD, Tay F, Sun J, et al. Self-healing adhesive with antibacterial activity in water-aging for 12 months. Dent Mater 2019;35:1104–16.
[7] Aminoroaya A, Esmaeely Neisiany R, Nouri Khorasani S, Panahi P, Das O, Ramakrishna S. A review of dental composites: methods of characterizations. ACS Biomate Sci Eng 2020;6:3713–44.
[8] Sharma A, Alam S, Sharma C, Patnaik A, Kumar SR. Static and dynamic mechanical behavior of microcapsule-reinforced dental composite. Proc Inst Mech Eng, P I Mech Eng L-J Mat 2017;233:1184–90.
[9] Wu J, Weir MD, Melo MA, Strassler HE, Xu HH. Effects of water-aging on self-healing dental composite containing microcapsules. J Dent 2016;47:86–93.
[10] Blaiszik BJ, Kramer SLB, Olugebefola SC, Moore JS, Sottos NR, White SR. Self-healing polymers and composites. Annu Rev Mater Res 2010;40:179–211.
[11] Ghorbanpour Arani A, Miralaei N, Farazin A, Mohammadimehr M. An extensive review of the repair behavior of smart self-healing polymer matrix composites. J Mater Res 2023;38:617–32.
[12] Chen J, Huang Y, Ma X, Lei Y. Functional self-healing materials and their potential applications in biomedical engineering. Adv Compos Hybrid Ma 2018;1:94–113.
[13] Kumar EK, Patel SS, Kumar V, Panda SK, Mahmoud SR, Balubaid M. State of art review on applications and mechanism of self-healing materials and structure. Arch Comput Method E 2023;30:1041–55.
[14] Sitnikov NN, Khabibullina IA, Mashchenko VI, Rizakhanov RN. Prospects of application of self-healing materials and technologies based on them. Inorg Mater Appl Res 2018;9:785–93.
[15] Del Prado-Audelo ML, Caballero-Florán IH, Mendoza-Muñoz N, Giraldo-Gomez D, Sharifi-Rad J, Patra JK, et al. Current progress of self-healing polymers for medical applications in tissue engineering. Iran Polym J 2022;31:7–29.
[16] Bekas DG, Tsirka K, Baltzis D, Paipetis AS. Self-healing materials: A review of advances in materials, evaluation, characterization and monitoring techniques. Compos Part B-Eng 2016;87:92–119.
[17] Mohd Kanafi N, Abdul Ghani A, Abdul Rahman N, Abd Aziz A, Sapuan SM. A review of self-healable natural rubber based on reversible bonds: fundamental, design principle and performance. J Mater Sci 2023;58:608–35.
[18] Chen K, Zhou J, Hu J, Zhang J, Heng T, Xu C, et al. Preparation of pH-responsive dual-compartmental microcapsules via pickering emulsion and their application in multifunctional textiles. ACS Appl Mater Inter 2021;13:1234–44.
[19] Jiang W, Zhou G, Duan J, Liu D, Zhang Q, Tian F. Synthesis and characterization of a multifunctional sustained-release organic–inorganic hybrid microcapsule with self-healing and flame-retardancy properties. ACS Appl Mater Inter 2021;13:15668–79.
[20] Zhu DY, Rong MZ, Zhang MQ. Self-healing polymeric materials based on microencapsulated healing agents: From design to preparation. Prog Polym Sci 2015;49–50:175–220.
[21] Liu J, Zheng N, Li Z, Liu Z, Wang G, Gui L, et al. Fast self-healing and antifouling polyurethane/fluorinated polysiloxane-microcapsules-silica composite material. Adv Compos Hybrid Ma 2022;5:1899–909.
[22] Zheng N, Liu J, Wang G, Yao P, Dang L, Liu Z, et al. Robust UV/moisture dual curable PDMS-microcapsule-silica functional material for self-healing, antifouling, and antibacterial applications. Nano Res 2023;16:7810–9.
[23] Gladman AS, Celestine A-DN, Sottos NR, White SR. Autonomic healing of acrylic bone cement. Adv Health Mater 2015;4:202–7.
[24] Zhang L, Ma Z, Wang R, Zhu M. Synthesis and characterization of methacrylate-functionalized betulin derivatives as antibacterial comonomer for dental restorative resins. ACS Biomate Sci Eng 2021;7:3132–40.
[25] Liang J, Liu F, Zou J, Xu HHK, Han Q, Wang Z, et al. pH-responsive antibacterial resin adhesives for secondary caries inhibition. J Dent Res 2020;99:1368–76.
[26] Hu C, Wang L-L, Lin Y-Q, Liang H-M, Zhou S-Y, Zheng F, et al. Nanoparticles for the treatment of oral biofilms: current state, mechanisms, influencing factors, and prospects. Adv Health Mater 2019;8:1901301.
[27] Wu J, Weir MD, Melo MA, Xu HH. Development of novel self-healing and antibacterial dental composite containing calcium phosphate nanoparticles. J Dent 2015;43:317–26.

[28] Chi M, Qi M, A L, Wang P, Weir MD, Melo MA, et al. Novel bioactive and therapeutic dental polymeric materials to inhibit periodontal pathogens and biofilms. Plos One 2019;20:278.
[29] Wu J, Zhang Q, Zhu T, Ge J, Zhou C. Development of novel self-healing and antibacterial resin composite containing microcapsules filled with polymerizable healing monomer. Chin J Stomatol 2015;50:469–73.
[30] Hu G, Zhang XY, Zhao JX, Zhou CJ, Wu JL. Development of novel self-adhesive resin cement with antibacterial and self-healing properties. West China J Stomatol 2020;38:256–62.
[31] Yue S, Wu J, Zhang Q, Zhang K, Weir MD, Imazato S, et al. Novel dental adhesive resin with crack self-healing, antimicrobial and remineralization properties. J Dent 2018;75:48–57.
[32] Chen C, Wu J, Weir MD, Wang L, Zhou X, Xu HHK, et al. Dental Composite Formulation Design with Bioactivity on Protein Adsorption Combined with Crack-Healing Capability. J Funct Biomater 2017;8:40.
[33] Ahangaran F, Navarchian AH. Towards the development of self-healing and antibacterial dental nanocomposites via incorporation of novel acrylic microcapsules. Dent Mater 2022;38:858–73.
[34] Zhou X, Li WP, Zhu LQ, Ye H, Liu HC. Polymer-silica hybrid self-healing nano/microcapsules with enhanced thermal and mechanical stability. RSC Adv 2019;9:1782–91.
[35] Caruso MM, Blaiszik BJ, Jin H, Schelkopf SR, Stradley DS, Sottos NR, et al. Robust, Double-Walled Microcapsules for Self-Healing Polymeric Materials. ACS Appl Mater Inter 2010;2:1195–9.
[36] Li Q, Mishra AK, Kim NH, Kuila T, Lau K-t, Lee JH. Effects of processing conditions of poly(methylmethacrylate) encapsulated liquid curing agent on the properties of self-healing composites. Compos Part B-Eng 2013;49:6–15.
[37] Wang Y, Cheng Q, Liu J, Tariq Z, Zheng Z, Li G, et al. Tuning microcapsule shell thickness and structure with silk fibroin and nanoparticles for sustained release. ACS Biomate Sci Eng 2020;6:4583–94.
[38] Yao S, Qin L, Wang Z, Zhu L, Zhou C, Wu J. Novel nanoparticle-modified multifunctional microcapsules with self-healing and antibacterial activities for dental applications. Dent Mater 2022;38:1301–15.
[39] Wang Y, Hua H, Li W, Wang R, Jiang X, Zhu M. Strong antibacterial dental resin composites containing cellulose nanocrystal/zinc oxide nanohybrids. J Dent 2019;80:23–9.
[40] Zhang J, Chen C, Chen J, Zhou S, Zhao Y, Xu M, et al. Dual Mode of Anti-Biofilm Action of G3 against Streptococcus mutans. ACS Appl Mater Inter 2020;12:27866–75.
[41] Luo D, Shahid S, Sukhorukov GB, Cattell MJ. Synthesis of novel chlorhexidine spheres with controlled release from a UDMA–HEMA resin using ultrasound. Dent Mater 2017;33:713–22.
[42] Imazato S, Kinomoto Y, Tarumi H, Torii M, Russell RRB, McCabe JF. Incorporation of Antibacterial Monomer MDPB into Dentin Primer. J Dent Res 1997;76:768–72.
[43] Zhao Z, Ma X, Chen R, Xue H, Lei J, Du H, et al. Universal Antibacterial Surfaces Fabricated from Quaternary Ammonium Salt-Based PNIPAM Microgels. ACS Appl Mater Inter 2020;12:19268–76.
[44] Wu J, Zhou H, Weir MD, Melo MAS, Levine ED, Xu HHK. Effect of dimethylaminohexadecyl methacrylate mass fraction on fracture toughness and antibacterial properties of CaP nanocomposite. J Dent 2015;43:1539–46.
[45] Ishihara K., Nomura H., Mihara T., Kurita K., Iwasaki Y., Nakabayashi N. Why do phospholipid polymers reduce protein adsorption? J. Biomed Mater Res. 8;39:323–330.
[46] Zhang N, Ma J, Melo MAS, Weir MD, Bai Y, Xu HHK. Protein-repellent and antibacterial dental composite to inhibit biofilms and caries. J Dent 2015;43:225–34.
[47] Jain A, Duvvuri LS, Farah S, Beyth N, Domb AJ, Khan W. Antimicrobial Polymers. Adv Health Mater 2014;3:1969–85.
[48] Song Y-K, Chung C-M. Repeatable self-healing of a microcapsule-type protective coating. Polym Chem 2013;4:4940–7.
[49] Wang Z, Zhang X, Yao S, Zhao J, Zhou C, Wu J. Development of low-shrinkage dental adhesives via blending with spiroorthocarbonate expanding monomer and unsaturated epoxy resin monomer. J Mech Behav Biomed Mater 2022;133:105308.
[50] Song F, Koo H, Ren D. Effects of material properties on bacterial adhesion and biofilm formation. J Dent Res 2015;94:1027–34.
[51] Li H, Wang R, Hu H, Liu W. Surface modification of self-healing poly(urea-formaldehyde) microcapsules using silane-coupling agent. Appl Surf Sci 2008;255:1894–900.
[52] Kitamura K. Effect of bacteriocin productive streptococcus mutans strain on infection and establishment of S. mutans. Jpn J Pedia Dent 1985;23:153–77.
[53] van der Hoeven JS, Rogers AH. Stability of the resident microflora and the bacteriocinogeny of Streptococcus mutans as factors affecting its establishment in specific pathogen-free rats. Infect Immun 1979;23:206–13.
[54] Namba N, Yoshida Y, Nagaoka N, Takashima S, Matsuura-Yoshimoto K, Maeda H, et al. Antibacterial effect of bactericide immobilized in resin matrix. Dent Mater 2009;25:424–30.
[55] Campos KdPL, Viana GM, Cabral LM, Portela MB, Hirata Junior R, Cavalcante LM, et al. Self-cured resin modified by quaternary ammonium methacrylates and chlorhexidine: Cytotoxicity, antimicrobial, physical, and mechanical properties. Dent Mater 2020;36:68–75.
[56] Imazato S, Russell RRB, McCabe JF. Antibacterial activity of MDPB polymer incorporated in dental resin. J Dent 1995;23:177–81.
[57] Brosh T, Ganor Y, Belov I, Pilo R. Analysis of strength properties of light-cured resin composites. Dent Mater 1999;15:174–9.
[58] Ahangaran F, Hayaty M, Navarchian AH, Pei Y, Picchioni F. Development of self-healing epoxy composites via incorporation of microencapsulated epoxy and mercaptan in poly(methyl methacrylate) shell. Polym Test 2019;73:395–403.
[59] Zhang H, Wang P, Yang J. Self-healing epoxy via epoxy–amine chemistry in dual hollow glass bubbles. Compos Sci Technol 2014;94:23–9.
[60] Abid Althaqafi K, Alshabib A, Satterthwaite J, Silikas N. Properties of a model self-healing microcapsule-based dental composite reinforced with silica nanoparticles. J Funct Biomater 2022;13:19.
[61] Brown EN, White SR, Sottos NR. Microcapsule induced toughening in a self-healing polymer composite. J Mater Sci 2004;39:1703–10.
[62] Wu J, Zhang Q, Weir MD, Oates TW, Zhou C, Chang X, et al. Novel self-healing dental luting cements with microcapsules for indirect restorations. J Dent 2017;66:76–82.